Velocity Error for Coherent Doppler Lidar with Pulse Accumulation*

ROD FREHLICH

Cooperative Institute for Research in the Environmental Sciences, University of Colorado, Boulder, Colorado

(Manuscript received 23 July 2003, in final form 1 December 2003)

ABSTRACT

The random estimation or instrument error of coherent Doppler lidar velocity estimates with pulse accumulation (multiple lidar shots per velocity estimate) is determined with computer simulations for general conditions. The sampling errors for overlaid lidar tracks and tropospheric wind field conditions are also calculated for space-based operation. These results permit useful engineering analysis based on the total observation error of the velocity measurements.

1. Introduction

Coherent Doppler lidar is an attractive instrument for the global measurements of winds from a space-based platform (Baker et al. 1995; Huffaker et al. 1984; Huffaker and Hardesty 1996; Menzies 1986; Menzies and Hardesty 1989). The impact of Doppler lidar and other future data products can be determined using observing system simulation experiments (OSSEs). Several OSSEs have investigated the impact of global winds using a space-based Doppler lidar (Atlas 1997; Baker et al. 1995; Rohaly and Krishnamurti 1993). A complete statistical description of the velocity measurements is required to evaluate the impact of these new data products, to perform comparisons with alternative measurements, and to improve the engineering designs and signal processing for future measurements from space.

Ground-based coherent Doppler lidars have been operated for many years to measure wind fields and wind field statistics (Frehlich et al. 1994, 1998; Huffaker and Hardesty 1996; Menzies and Hardesty 1989). The development of solid-state coherent Doppler lidars (Henderson et al. 1991, 1993; Kavaya et al. 1989) has produced higher efficiency and performance. A short laser pulse is transmitted as a small collimated beam and the photons scattered by aerosol particles are collected by a telescope, focused onto a detector, and mixed with a frequency-stable laser reference beam called a local oscillator (LO). This coherent or heterodyne detection process is a very sensitive technique and therefore is attractive for space-based applications where power and weight are a premium. The radial velocity v_r of the aerosol particles produces a Doppler frequency shift f given by

$$v_r = \lambda f/2, \tag{1}$$

where λ is the wavelength of the laser. For a 2-μm laser pulse, 1 m s^{-1} of radial velocity corresponds to a 1-MHz Doppler frequency shift, which can be estimated as the pulse travels through the atmosphere. The detector bandwidth is determined by the maximum observable velocity (typically 100–200 m s^{-1}), which is very small compared with the laser frequency, and therefore the contribution of background solar light is negligible. The performance of velocity estimates depends on the final processing velocity search space v_{search}. For the purpose of computer simulations of performance, complex coherent Doppler lidar data are generated with a sampling interval T_S given by

$$v_{\text{search}} = \lambda/(2T_S). \tag{2}$$

A Doppler lidar produces estimates of the radial component or line of sight (LOS) of the velocity vector averaged over the sampling volume of the measurement. The statistical properties of the coherent Doppler lidar signal produce a unique behavior of the velocity measurements. When the signal level is high, the velocity estimates are unbiased and the error is usually determined by the wind variability over the measurement volume. When the signal level is low, the random fluctuations of the signal compete with the detector noise fluctuations and produce two types of estimates: the good estimates located around the true average velocity and the bad estimates that are distributed uniformly over the velocity search space v_{search} (Frehlich et al. 1994, 1997). This statistical behavior is conveniently described by the fraction b of bad estimates and the stan-

* Supplemental material related to this paper is available at the Journals Online Web site: http://dx.doi.org/10.1175/JTECH1596supl1.

Corresponding author address: Dr. Rod Frehlich, CIRES, Campus Box 216, University of Colorado, Boulder, CO 80309.
E-mail: rgf@cires.colorado.edu

© 2004 American Meteorological Society

Unauthenticated | Downloaded 09/28/21 01:45 AM UTC

dard deviation g or rms error of the good estimates. The parameters b and g can be determined with computer simulations (Frehlich 1996, 1997, 2000, 2001b) and from analysis of actual lidar data (Frehlich et al. 1994, 1997).

Profiles of the horizontal vector winds are produced by scanning the lidar beam or stepping the lidar beam through a sequence of different angles or perspectives (step stare). The first design for space-based measurements proposed a conical scan (Baker et al. 1995; Huffaker et al. 1984), which requires a high-power laser to produce acceptable signal levels for every laser shot. Performance is improved by fixing the laser beam and accumulating the signal from many lidar shots for each range gate (Frehlich and Yadlowsky 1994; Frehlich 1996, 1997; Frehlich et al. 1997, 1998; Rye and Hardesty 1993a,b). This also improves the spatial averaging of the wind estimates and reduces the threshold signal energy required for a good estimate. In many cases, the wind variability over the measurement volume determines the performance of the velocity estimates and a full statistical description of the wind field is required to predict coherent Doppler lidar performance. In addition, the statistical variations of the atmospheric aerosol backscatter (Belan 1987; Osipenko et al. 1989; Bowdle 1997) should also be included (Frehlich 2000).

There are a number of parameters that affect the performance of the velocity estimates. These include the laser wavelength, the transmitted pulse width, the pulse repetition frequency, the pulse energy, the velocity search space v_{search}, the range-gate length Δp, the number N of shots accumulated per velocity estimate, the spatial separation between laser shots, the atmospheric variations of velocity and backscatter, the random pointing errors of the lidar beam, and the random errors in the reference velocity. The threshold signal level is defined by the number of photons required to produce a given fraction b of random outliers. When the number of received photons is high, there are no random outliers ($b = 0$) and the velocity error g is typically very accurate and more accurate than the data requirements (Frehlich 2001a). Therefore, the critical parameter regime is the weak-signal regime defined by $0.001 < b < 0.5$. The performance of the threshold signal level and the accuracy of the good estimates as a function of N is well described by simple scaling laws (Frehlich 1996), especially for larger N, which is typical for space-based measurements. Here we produce empirical functions for the performance of the Capon velocity estimator for the weak-signal regime as a function of all the important input parameters. The better velocity estimators have similar performance to the Capon estimator, especially for the fraction of random outliers (Frehlich 1996).

For spaced-based measurements of the profile of horizontal velocity, the most promising lidar beam scanning geometry is overlaid forward and aft tracks. This geometry produces the most robust LOS measurements and therefore the most robust horizontal vector measurements. The two orthogonal components (u, v) of the horizontal velocity vector are chosen as the along-track component (u) and the across-track component (v). The measurement ($\hat{u}$, $\hat{v}$) of the horizontal velocity velocity (u, v) is produced in terms of the lidar beam angles and the forward and aft LOS radial velocity measurements. The total random error of the u velocity component is given by (Frehlich 2001a)

$$\Sigma_u^2 = \langle [\hat{u} - u_{\text{truth}}]^2 \rangle = \delta_u^2 + \sigma_u^2, \tag{3}$$

where δ_u is the magnitude of the sampling or error of representativeness and σ_u is the magnitude of the random error from the LOS measurements. Similarly, for the v velocity component,

$$\Sigma_v^2 = \langle [\hat{v} - v_{\text{truth}}]^2 \rangle = \delta_v^2 + \sigma_v^2. \tag{4}$$

Here, (u_{truth}, v_{truth}) is the desired horizontal vector measurement, which is defined as the average of the random horizontal velocity (u, v) over the measurement volume, which is typically chosen as the dimensions of the appropriate numerical model grid cell. The sampling errors δ_u and δ_v are a measure of how well the lidar scanning pattern samples the total measurement volume. The sampling error therefore depends on the scanning pattern and the statistical description of the random velocity field. Calculations of the sampling error have been presented by Frehlich (2001a) for various instruments and atmospheric conditions. These results will be extended to the overlaid step-stare beam geometry of arbitrary track length.

2. Lidar parameters

The performance of Doppler lidars depends on the lidar parameters, the atmospheric conditions, and the velocity estimation algorithm. The transmitted pulse for a solid-state lidar is well approximated as a Gaussian temporal power profile with a full-width at half-maximum (FWHM) pulse width Δt (Frehlich et al. 1994, 1997). The illuminated aerosol target region is a narrow pencil-shaped volume that has a Gaussian intensity profile along the beam axis with a spatial width (FWHM) $\Delta r = \Delta tc/2$, where c is the speed of light in air. The line-of-sight range-gate length $\Delta p = Tc/2$ is defined as the distance the illuminated aerosol region travels during the data processing interval $T = MT_S$, where M is the number of complex lidar data points for each range gate. For pulse accumulation the along-track extent of the measurement volume $L_{\text{track}} = \Delta xN$, where N is the number of accumulated pulses and Δx is the horizontal separation between adjacent lidar shots. To simplify the numerical simulations, we assume the lidar beam axis is perpendicular to the satellite track with a nadir angle θ, where $\theta = 0$ is pointed to the center of the earth.

For a short range gate located at range R and for an

Unauthenticated | Downloaded 09/28/21 01:45 AM UTC

aerosol target with constant aerosol backscatter coefficient $\beta(R)$, the magnitude of the return Doppler lidar signal for one lidar shot is defined by the parameter (Frehlich and Yadlowsky 1994; Frehlich 1996)

$$\Phi_1 = \frac{\eta_Q \beta(R) K(R)^2 c U_T A_R \eta_H T}{2h\nu R^2}, \quad (5)$$

where η_Q is the detector quantum efficiency, $K(R)$ is the one-way irradiance extinction, U_T is the transmitted laser pulse energy, A_R is the receiver area, η_H is the heterodyne efficiency, h is Planck's constant, and ν is the laser frequency. Note that Φ_1 is the effective number of coherent photons detected per range gate per shot (Frehlich and Yadlowsky 1994). The most important atmospheric contribution to signal energy is the backscatter coefficient $\beta(R)$ and extensive efforts have been made to characterize its global statistical distribution (Rothermel et al. 1989, 1996; Bowdle 1997).

For the ideal case of constant velocity and backscatter over a short range gate compared with the range R, the Doppler lidar signal spectrum $S(f)$ is Gaussian $\{S(f) \propto \exp[-f^2/(2w^2)]\}$ and the spectral width w is given in terms of the pulse width as (Frehlich 1993)

$$w = \frac{(\ln 2/2)^{1/2}}{\pi \Delta t} = \frac{0.187\ 390\ 6}{\Delta t}. \quad (6)$$

The spectral width w_v in velocity space [see Eq. (1)] is then

$$w_v = \lambda w/2. \quad (7)$$

The major instrumental error in the radial velocity is the frequency drift in the LO or reference laser that defines zero velocity. The effects of uncorrelated instrumental velocity error from shot to shot are included in the simulations by adding a zero-mean Gaussian random velocity error with an uncorrelated rms error (standard deviation) $\sigma_{v\,\mathrm{LO}}$ to the zero velocity reference of each shot. The case of correlated random error is a simple extension.

3. General atmospheric parameters

For space-based lidar measurements the radial velocity $v_r(x, r)$ is given by

$$\begin{aligned} v_r(x, r) = {} & u[x(r), y(r), z(r)] \cos\phi \sin\theta \\ & + v[x(r), y(r), z(r)] \sin\phi \sin\theta \\ & - w[x(r), y(r), z(r)] \cos\theta, \end{aligned} \quad (8)$$

where

$$x(r) = r \sin\theta \cos\phi, \quad (9)$$

$$y(r) = r \sin\theta \sin\phi, \quad \text{and} \quad (10)$$

$$z(r) = -r \cos\theta \quad (11)$$

are the Cartesian coordinates as a function of the radial distance r along the lidar beam axis (see Fig. 1 of Frehlich 2001a). Here, θ is the zenith angle of the beam; ϕ is the azimuth angle of the beam; x is the distance along the satellite track; y is the distance transverse to the satellite track; z is the vertical coordinate; and $u(x, y, z)$, $v(x, y, z)$, and $w(x, y, z)$ are the along-track component, across-track component, and vertical component of the velocity field, respectively.

The radial velocity $v_r(x, r)$ over the measurement plane is a superposition of a mean radial velocity $V_r(x, r)$ and the zero-mean radial velocity fluctuations $v_r'(x, r)$, where r is the distance along the lidar beam axis. The mean radial velocity $V_r(x, r)$ includes a constant value V_0 and a shear component $v_{r\mathrm{shr}}$, which is assumed constant over the measurement volume vertical distance L_z and

$$v_{r\mathrm{shr}} = \cos\phi \sin\theta\, u_{\mathrm{shr}} + \sin\phi \sin\theta\, v_{\mathrm{shr}}, \quad (12)$$

where u_{shr} and v_{shr} are the vertical shear in the u and v components, respectively. A rigorous separation of the velocity fluctuations and shear is produced by defining the shear as the best-fit vertical shear of the desired velocity component over the measurement plane described by the lidar beam. For some applications, the shear is defined as the best fit over the measurement volume.

For homogeneous statistics, the zero-mean radial velocity fluctuations $v_r'(x, r)$ are described by the covariance function:

$$B_{vr}(x, r) = \langle v_r'(x_0, r_0) v_r'(x_0 + x, r_0 + r) \rangle, \quad (13)$$

where x is the lag in the direction of the satellite track and r is the lag along the lidar beam axis. Realizations of the radial velocity are generated numerically with the prescribed covariance $B_{vr}(x, r)$ (Frehlich 2000).

An important aspect of measurements over a random velocity field is the definition of the desired or true velocity measurement v_{truth}, which is required for the definition of error. A velocity estimate $\hat{v}$ is unbiased if $\langle \hat{v} - v_{\mathrm{truth}} \rangle = 0$ where $\langle\ \rangle$ denotes an ensemble average over many realizations of the wind field. This problem has been investigated for single-shot (Frehlich 1997) and multiple-shot (Frehlich 2000) lidar velocity estimates using computer simulations (Frehlich 1997). For high spatial resolution single-shot lidar measurements of the radial velocity, $v_{r\mathrm{truth}}$ was given by a pulse-weighted version of the random radial velocity. However, if the pulse volume Δr was much less than the range-gate dimensions Δp, then $v_{r\mathrm{truth}}$ is well approximated by the linear average of the radial velocity over the range-gate length Δp. Similarly, for the two-dimensional space-based multishot measurement we define the desired radial velocity measurement $v_{r\mathrm{truth}}$ as the linear average of the radial velocity over the measurement plane A; that is,

$$v_{r\mathrm{truth}} = \frac{1}{A} \int_A v_r(x, r)\, dx\, dr. \quad (14)$$

In the same manner (Frehlich 1997), the average ve-

Unauthenticated | Downloaded 09/28/21 01:45 AM UTC

locity variability over the measurement plane A is defined as

$$s^2_{v\text{eff}} = \frac{1}{A}\int_A \langle [v_r(x, r) - v_{r\text{truth}}]^2\rangle \, dx \, dr, \quad (15)$$

which is the average squared difference between the radial velocity $v_r(x, r)$ and the desired mean velocity $v_{r\text{truth}}$.

If the velocity fluctuations $v'_r(x, r)$ are spatially homogeneous,

$$s^2_{v\text{eff}} = s^2_{\text{shr}} + s^2_{vr}, \quad (16)$$

where

$$s^2_{\text{shr}} = \frac{v^2_{r\text{shr}}(\Delta p)^2}{12} = \frac{(\cos^2\phi \sin^2\theta \, u^2_{\text{shr}} + \sin^2\phi \sin^2\theta \, v^2_{\text{shr}})(\Delta p)^2}{12} \quad (17)$$

is the contribution from the vertical shear and

$$s^2_{vr} = \frac{1}{A}\int_A \langle [v'_r(x, r) - v'_{r\text{ave}}]^2\rangle \, dx \, dr \quad (18)$$

is the contribution from turbulence where

$$v'_{r\text{ave}} = \frac{1}{A}\int_A v'_r(x, r) \, dx \, dr. \quad (19)$$

If the observation plane A is a rectangle with dimensions L_x and L_r, then

$$s^2_{vr} = \frac{2}{L_r L_x}\int_0^{L_x}\int_0^{L_r}\left(1 - \frac{r}{L_r}\right)\left(1 - \frac{x}{L_x}\right)D_{vr}(x, r) \, dr \, dx, \quad (20)$$

where $D_{vr}(x, r)$ is the structure function of the radial velocity fluctuations $v'_r(x, r)$; that is,

$$D_{vr}(x, r) = \langle [v'_r(x_0, r_0) - v'_r(x_0 + x, r_0 + r)]^2\rangle = 2[B_{vr}(0, 0) - B_{vr}(x, r)], \quad (21)$$

where the ensemble average is performed over statistically similar atmospheres.

If the radial velocity fluctuations along the lidar axis are negligible compared with the fluctuations along the lidar track, then

$$s^2_{vr} = \frac{1}{L_{\text{track}}}\int_0^{L_{\text{track}}}\left(1 - \frac{x}{L_{\text{track}}}\right)D_{vr}(x) \, dx, \quad (22)$$

where L_{track} is the length of the lidar track and $D_{vr}(x) = D_{vr}(x, 0)$ is the structure function of the radial velocity along the lidar track at the center of the measurement cell. Note that Eqs. (20) and (22) require a complete statistical description of the velocity field because the radial velocity Eq. (8) is a function of all three components of the velocity field.

A common approximation for including the effects of wind variability is the use of an effective Gaussian pulse and constant backscatter and constant velocity over the measurement volume. The heterodyne lidar signal spectrum $S(f)$ is then a Gaussian function with an effective spectral width in velocity space $w_{v\text{eff}}$ given by [see Eqs. (6) and (7)]

$$w^2_{v\text{eff}} = s^2_{vr} + s^2_{\text{shr}} + w^2_v + \sigma^2_{v\text{LO}} \quad (23)$$

and is related to the effective spectral width w_{eff} by

$$w_{v\text{eff}} = \lambda w_{\text{eff}}/2, \quad (24)$$

and the parameter

$$\Omega = w_{\text{eff}} M T_S = 2 w_{v\text{eff}} M T_S/\lambda \quad (25)$$

is a basic performance parameter (Frehlich and Yadlowsky 1994).

The random variations in aerosol backscatter $\beta(x, r)$ over the measurement plane A can be included in the analysis by defining

$$\Phi_1 = \frac{\eta_Q \beta_A K(R)^2 c U_T A_R \eta_H T}{2h\nu R^2}, \quad (26)$$

where

$$\beta_A = \frac{1}{A}\int_A \beta(x, r) \, dr \, dx \quad (27)$$

is the average of the backscatter $\beta(x, r)$ over the measurement plane A. The statistical properties of Φ_1 are determined by the spatial statistics of backscatter $\beta(x, r)$ (Belan 1987; Osipenko et al. 1989; Bowdle 1997; Frehlich 2000). Therefore, the metric Φ_1 is a random variable for each lidar measurement.

4. Atmospheric parameters for space-based measurements

One of the most promising lidar beam geometries for space-based measurements of winds is two overlaid lidar tracks located forward and aft of the satellite track (Frehlich 2001a). The pulse accumulation of the multiple lidar shots increases the sensitivity and improves the sampling of the desired measurement volume. Simple expressions for the contribution of wind variability can be produced by assuming the shear is the dominant contribution in the radial direction and that turbulence is the dominate contribution along the lidar track. If one assumes that the fluctuations in u, v, and w are uncorrelated, then

$$s^2_{vr} = \cos^2\phi \sin^2\theta s^2_u + \sin^2\phi \sin^2\theta s^2_v + \cos^2\theta s^2_w, \quad (28)$$

where

$$s^2_i = \frac{1}{L_{\text{track}}}\int_0^{L_{\text{track}}}\left(1 - \frac{x}{L_{\text{track}}}\right)D_i(x) \, dx, \quad (29)$$

where $D_i(x)$ is the structure function of the velocity component i in the satellite track direction x.

Unauthenticated | Downloaded 09/28/21 01:45 AM UTC

a. Tropospheric conditions

The spatial statistics of the horizontal wind field in the troposphere are well approximated by a Kolmogorov spatial spectrum. However, the along-track and across-track velocity components are not exactly consistent with the predictions of two- or three-dimensional isotropic turbulence (Lindborg 1999). For three-dimensional isotropic Kolmogorov tropospheric conditions (Frehlich 2001a),

$$s_u^2 = \frac{9}{20}(\epsilon L_{\text{track}})^{2/3} \quad \text{and} \tag{30}$$

$$s_v^2 = \frac{3}{5}(\epsilon L_{\text{track}})^{2/3}, \tag{31}$$

where ϵ is the energy dissipation rate. The contributions s_w from the vertical velocity fluctuations are typically negligible.

b. Atmospheric boundary layer conditions

Boundary layer wind field statistics are more complex than tropospheric conditions. The von Kármán spatial spectrum is a simple two-parameter model described by the variance σ_x^2 and the integral length scale L_{ix} for each velocity component x (Frehlich 2001a). If $L_{ix} \ll L_{\text{track}}$,

$$s_u^2 = \sigma_u^2\left(1 - 2\frac{L_{iu}}{L_{\text{track}}} + 2.390\,051\frac{L_{iu}^2}{L_{\text{track}}^2}\right), \tag{32}$$

$$s_v^2 = \sigma_v^2\left(1 - \frac{L_{iv}}{L_{\text{track}}}\right), \quad \text{and} \tag{33}$$

$$s_w^2 = \sigma_w^2\left(1 - \frac{L_{iw}}{L_{\text{track}}}\right), \tag{34}$$

where the von Kármán model is substituted into Eq. (29) and simplified assuming $L_{ix} \ll L_{\text{track}}$. In practice, more complex models for the boundary layer statistics may be required for accurate estimates under realistic conditions.

5. Performance of Doppler lidar velocity estimates

The performance of coherent Doppler lidar velocity estimates can be determined for realistic atmospheric conditions with careful computer simulations (Frehlich 2000). The mean velocity $V(x, r)$ and the random radial velocity $v_r'(x, r)$ are used to simulate the Doppler lidar signal for N lidar shots. The random radial velocity for lidar pulse number i is $v_r(i\Delta x, r)$. Raw lidar data are generated using a Monte Carlo technique (Frehlich 1997, 2000; Salamitou et al. 1995). The variations in backscatter over the range gate have a small effect on velocity estimator performance (Rye 1990). Shot-to-shot backscatter variability is added using simulations of aerosol backscatter $\beta(y)$ that satisfies a von Kármán spatial spectrum with a standard deviation that is 50% of the mean. The N shots of simulated data are processed with the Capon velocity estimator using the accumulated signal covariance (Anderson 1991; Frehlich 1996, 1997; Frehlich and Yadlowsky 1994; Marple 1987; Rye and Hardesty 1993a,b). This robust estimator was proposed by Anderson (1991) for space-based coherent Doppler lidars. The Capon estimator is a minimum variance spectral estimator that is implemented using the biased covariance estimates of the complex data and the Yule–Walker solution for the autoregressive coefficients (Marple 1987, p. 357). Optimal performance of the Capon estimator requires the selection of an autoregressive filter order o. To determine the statistical behavior of the lidar velocity estimates with acceptable accuracy, 80 000 realizations of the wind field and velocity estimates were generated.

The performance of the Doppler lidar estimates $\hat{v}$ of the radial velocity v is described by the probability density function (PDF). An important issue for space-based measurements is the performance of the velocity estimates in weak signal regimes where the PDF has a uniform distribution of random outliers and a localized distribution of good estimates with mean value v_g and rms error (standard deviation) g. The bias Δv of the good estimates of the measurement is

$$\Delta v = \langle v_{\text{truth}} - v_g \rangle. \tag{35}$$

For typical space-based conditions and the better velocity estimators the bias is zero (Frehlich 2001a).

The magnitude σ_e of the total random error of the radial velocity measurements with pulse accumulation for a velocity search space centered at v_0 is then

$$\sigma_e^2 = b(d^2 + v_{\text{search}}^2/12) + (1 - b)g^2, \tag{36}$$

where $d = v_0 - v_{\text{truth}}$ and $\sigma_e^2 = \langle(\hat{v} - v_{\text{truth}})^2\rangle$. In most cases, especially for space-based measurements, d will be random and

$$\sigma_e^2 = b(\langle d^2\rangle + v_{\text{search}}^2/12) + (1 - b)g^2, \tag{37}$$

where $\langle\ \rangle$ denotes the ensemble average over the realizations of d, which depends on the PDF of d. For assimilation of space-based measurements the PDF of d is determined by the first guess of the data assimilation algorithm (Atlas 1997). When the lidar signal level is high enough, there are no random outliers ($b = 0$) and $\sigma_e = g$. For space-based lidar measurements with overlaid forward and aft tracks and with equal and uncorrelated zero-mean radial velocity error of magnitude σ_e, the random errors of the estimates of the u and v components are also uncorrelated with magnitude [Frehlich (2001a), his Eqs. (73) and (74)]:

$$\sigma_u^2 = \frac{\sigma_e^2}{2\cos^2\phi\sin^2\theta} \quad \text{and} \tag{38}$$

$$\sigma_v^2 = \frac{\sigma_e^2}{2\sin^2\phi\sin^2\theta}. \tag{39}$$

Unauthenticated | Downloaded 09/28/21 01:45 AM UTC

The instrument and estimation errors σ_u and σ_v are important components of the total observation error Σ_u in Eq. (3) and Σ_v in Eq. (4).

The fraction of outliers b, the bias of the good estimates Δv, and the rms error g of the good estimates are calculated from simulated data using the algorithms described in appendix E of Frehlich (1997). The results are fit to empirical models such as

$$b(\Phi_1) = \exp(-\Phi_1^\alpha/b_0^\alpha), \quad (40)$$

$$b(\Phi_1) = \exp[-\exp(c_1 + c_2 \ln\Phi_1 + c_3 \ln^2\Phi_1)], \quad (41)$$

and

$$g(\Phi_1) = \chi[1 + (\Phi_1/g_0)^\gamma]^{-\delta} + \mu, \quad (42)$$

where the parameters α, b_0, c_i, χ, g_0, γ, δ, and μ are determined by standard best-fit algorithms (Press et al. 1986).

Equation (40) can be written as a linear function of $y = \ln[-\ln(b)]$ versus $x = \ln(\Phi_1)$, that is,

$$\ln[-\ln(b)] = \ln(\Phi_1^\alpha/b_0^\alpha) = -\alpha \ln b_0 + \alpha \ln(\Phi_1) \quad (43)$$

and the coefficients can be determined from the best-fit straight line of y versus x. Similarly, Eq. (41) can be written as

$$\ln[-\ln(b)] = c_1 + c_2 \ln\Phi_1 + c_3 \ln^2\Phi_1, \quad (44)$$

and the coefficients c_i can be determined from the best-fit parabola of $y = \ln[-\ln(b)]$ versus $x = \ln\Phi_1$.

The parameter Φ_1 is an average of the effective number of photons detected for each lidar shot and each range gate (Frehlich and Yadlowsky 1994). The backscatter coefficient $\beta(x, r)$ is the key atmospheric component of the signal energy Φ_1. The Capon filter order o is chosen by the minimum rms error g. Typically, $p = 1$ for large Φ_1 and slowly increases when random outliers appear. The bias Δv for all the simulations was not statistically different from zero. An example of the performance from a full atmospheric simulation and the effective Gaussian approximation is shown in Fig. 1.

Based on many simulations with various parameters there are three key results.

1) The optimal order in the weak signal regime is independent of Φ_1 and the number N of pulses accumulated.
2) The fraction of outliers and the standard deviation of the good estimates in the weak signal regime are approximately the same for the full simulation and the effective Gaussian model.
3) The standard deviation of the good estimates is approximately constant at high signal levels and therefore can be bounded by its value in the weak signal regime.

While the lower bound on the total velocity error is typically determined by atmospheric variability in the high-signal regime, the upper bound is determined by the velocity search space in the low-signal regime where the number of outliers is large.

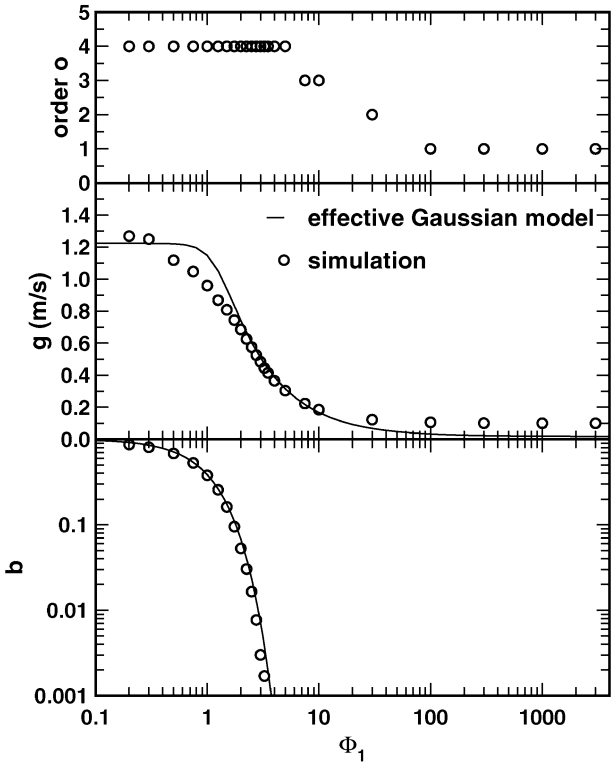

FIG. 1. Performance of Capon velocity estimator (○) for a full atmospheric simulation with optimal order o, rms error g of the good estimates, and fraction b of the bad estimates vs signal strength Φ_1 [Eq. (5)]. The best-fit models (-) [Eqs. (40) and (42)] are also shown for the results of the effective Gaussian model. The $1 - \sigma$ error bars for g and b are smaller than the symbols. The effective radial velocity variations from the lidar pulse, $w_v = 0.374\,79$ m s^{-1}; from turbulence, $s_{tr} = 0.733\,52$ m s^{-1}; from wind shear, $s_{shr} = 1.1482$ m s^{-1}; and from the shot-to-shot random LO error, $\sigma_{v\,LO} = 0.5$ m s^{-1}; the total effective signal spectral width, $w_{veff} = 1.4990$ m s^{-1}; and $\Omega = 11.242$. The Capon estimates were produced from $N = 100$ lidar shots, $M = 150$ complex data points per range gate, a sampling interval $T_S = 0.05$ μs, and a range-gate length $\Delta p = 1.1250$ km.

The optimal order o is determined empirically by simulations of performance for the weak signal regime. An approximation for the optimal order is

$$\sigma(\Omega, M) = \frac{p_1 M}{\Omega}(1 + p_2 \ln M + p_3 \ln\Omega + p_4 \ln M \ln\Omega), \quad (45)$$

where $p_1 = 0.218\,190$, $p_2 = 0.058\,689\,5$, $p_3 = 0.126\,683$, and $p_4 = -0.018\,290\,1$.

6. Parameters for general conditions in the weak signal regime

A careful choice of parameters is required to produce simple expressions for general lidar and atmospheric conditions. The weak signal regime is most critical for space-based applications because it defines the threshold

Unauthenticated | Downloaded 09/28/21 01:45 AM UTC

TABLE 1. Lidar simulation parameters.

Ω	M	Ω	M	Ω	M	Ω	M
0.25	12	1.00	24	2.00	400	8.00	200
0.25	24	1.00	50	4.00	30	8.00	400
0.25	50	1.00	100	4.00	50	16.00	120
0.50	12	1.00	200	4.00	100	16.00	200
0.50	24	2.00	24	4.00	200	16.00	400
0.50	50	2.00	50	4.00	400	32.00	400
0.50	100	2.00	100	8.00	60	32.00	800
1.00	12	2.00	200	8.00	100		

signal energy and the largest random error. The performance of Doppler lidar velocity estimates will be determined by the effective Gaussian model because it is numerically efficient and produces essentially the same performance for general atmospheric conditions. In addition, the number of parameters in the problem is reduced because the effective spectral width $w_{v\text{eff}}$ contains the contribution from the lidar pulse, the velocity shear and velocity turbulence, and the random LO shot-to-shot error.

The performance of the Doppler lidar velocity estimates is defined by the two functions $b(\Phi_1)$ (fraction of bad estimates) and $g(\Phi_1)$ (rms error of good estimates) for the N lidar pulses accumulated for each velocity estimate. The fraction b of random outliers is the most critical parameter and it defines the threshold signal level $\Phi_{1\text{thr}}$ by

$$b(\Phi_{1\text{thr}}) = b_{\text{thr}}, \tag{46}$$

where b_{thr} is the fraction of bad estimates at the threshold. For system design studies, the critical questions are the signal energy and the accuracy of the good velocity estimates at a specified threshold b_{thr}, that is, $\Phi_{1\text{thr}}(b_{\text{thr}})$ and $g(b_{\text{thr}})$. The performance for general conditions is given by empirical functions for $\Phi_{1\text{thr}}(b_{\text{thr}})$ and $g(b_{\text{thr}})$ for various values of b_{thr}. The performance curves $b(\Phi_1)$ and $g(\Phi_1)$ can then be recovered by interpolation or using a best-fit model.

The required input parameters for the simulation of performance are N, the number of lidar shots per estimate; M, the number of complex samples per range gate for each shot; $\Omega = w_{\text{eff}} MT_S$, the effective normalized spectra width; and $o(\Omega, M)$, the optimal filter order for the Capon estimator.

These four parameters are determined by the design parameters of the fixed LOS lidar measurement. The chosen parameters for the simulations are listed in Table 1. For each set of parameters M and Ω, $N = 10$, 20, 50, 100, and 200 pulses were used in the simulations.

7. Results

The performance of Doppler lidar velocity estimates is described by the two functions $b(\Phi_1, M, \Omega, N)$ and $g(\Phi_1, M, \Omega, N)$. However, the empirical scaling laws are more efficient for the functions $\Phi_{1\text{thr}}(b_{\text{thr}}, M, \Omega, N)$ and $g(b_{\text{thr}}, M, \Omega, N)/w_{v\text{eff}}$. To improve the accuracy of the empirical functions, the parameter space was split into a low Ω ($0.25 < \Omega < 2.0$) case and a high Ω ($2.0 < \Omega < 32.0$) case. The empirical functions tested for goodness of fit included

$$\Phi_{1\text{thr}}(b_{\text{thr}}, M, \Omega, N) = A(b_{\text{thr}}, M, \Omega)N^{-0.5+B(b_{\text{thr}},M,\Omega)/N} \quad \text{and} \tag{47}$$

$$g(b_{\text{thr}}, M, \Omega, N)/w_{v\text{eff}} = C(b_{\text{thr}}, M, \Omega) + D(b_{\text{thr}}, M, \Omega)/N^{\rho}, \tag{48}$$

where $A(b_{\text{thr}}, M, \Omega)$, $B(b_{\text{thr}}, M, \Omega)$, $C(b_{\text{thr}}, M, \Omega)$, and $D(b_{\text{thr}}, M, \Omega)$ were fit to the functions

$$f_1(b_{\text{thr}}, M, \Omega) = a_1 + a_2 \ln M + a_3 \ln\Omega + a_4 \ln M \ln\Omega + a_5 \ln^2 M + a_6 \ln^2\Omega + a_7 \ln^2 M \ln^2\Omega, \tag{49}$$

$$f_2(b_{\text{thr}}, M, \Omega) = a_1 M^{a_2}\Omega^{a_3}(1 + a_4 \ln M + a_5 \ln\Omega + a_6 \ln M \ln\Omega), \quad \text{and} \tag{50}$$

$$f_3(b_{\text{thr}}, M, \Omega) = \exp(a_1 + a_2 \ln M + a_3 \ln\Omega + a_4 \ln M \ln\Omega + a_5 \ln^2 M + a_6 \ln^2\Omega + a_7 \ln^2 M \ln^2\Omega), \tag{51}$$

and the function with the minimum mean-squared relative error was selected. The chosen function f_k and the coefficients a_i are listed in Tables 2–9.

Scatterplots of the model predictions versus $\Phi_{1\text{thr}}(b_{\text{thr}}, M, \Omega, N)$ and $g(b_{\text{thr}}, M, \Omega, N)$ for $b_{\text{thr}} = 0.1$ are shown in Figs. 2 and 3, respectively. Typically, the statistical accuracy of the estimates for $\Phi_{1\text{thr}}$ is better than for $g(b_{\text{thr}})$. The overall accuracy of the empirical model is better than 1% for all of the parameter space.

8. User manual

a. Performance at threshold b_{thr}

There are many input variables for defining the lidar and atmospheric parameters. One possible procedure for calculating performance at a specified threshold b_{thr} is as follows for a lidar beam zenith angle $\theta = 45°$, azimuth angle $\phi = 90°$, shear in u component $u_{\text{shr}} = 0$, and shear in the v component $v_{\text{shr}} = 5.0$ m s^{-1} km^{-1} (the input parameters and resulting calculations are indicated by square brackets):

- select the wavelength [$\lambda = 2.0$ μm];
- select N, the number of lidar shots per estimate [$N = 100$];
- select the range-gate length [$\Delta p = 1.1250$ km];
- select the velocity search space [$v_{\text{search}} = 20$ m s^{-1}];
- calculate $T_S = \lambda/(2v_{\text{search}})$ [$T_S = 0.05$ μs];
- calculate $M = 2\Delta p/(cT_S)$ [$M = 150$];
- calculate the radial velocity shear $v_{r\text{shr}}$ from the vertical

Unauthenticated | Downloaded 09/28/21 01:45 AM UTC

TABLE 2. Coefficients for A (b_{thr}, M, Ω) for $0.25 < \Omega < 2.0$.

b_{thr}	k	a_1	a_2	a_3	a_4	a_5	a_6	a_7
0.7	3	−1.114 612	0.700 483	−0.156 881	0.074 570	−0.045 979	−0.006 060	−0.000 186
0.6	3	−0.579 671	0.582 481	−0.058 129	0.060 536	−0.037 287	0.003 891	−0.000 106
0.5	3	−0.195 986	0.512 620	−0.003 515	0.054 617	−0.033 167	0.008 271	0.000 032
0.4	3	0.157 289	0.442 021	0.052 055	0.047 094	−0.028 289	0.012 582	0.000 013
0.3	3	0.473 844	0.383 177	0.101 475	0.040 455	−0.024 412	0.017 984	−0.000 072
0.2	1	1.427 377	1.297 391	−0.142 484	0.459 751	−0.048 798	0.067 883	0.015 769
0.1	1	2.587 928	1.312 152	0.349 887	0.461 104	−0.053 191	0.187 035	0.016 031
0.09	1	2.752 629	1.311 677	0.421 518	0.460 365	−0.053 704	0.203 024	0.016 117
0.08	1	2.932 743	1.311 849	0.496 192	0.460 645	−0.054 535	0.217 197	0.016 524
0.07	1	3.141 983	1.307 166	0.577 582	0.460 907	−0.054 618	0.235 832	0.016 610
0.06	1	3.386 765	1.291 455	0.690 411	0.455 818	−0.053 247	0.263 792	0.016 349
0.05	1	3.644 024	1.290 032	0.805 602	0.454 008	−0.054 168	0.289 876	0.016 482
0.04	1	4.020 670	1.256 049	0.965 470	0.445 292	−0.051 277	0.324 821	0.016 332
0.03	3	1.595 790	0.174 217	0.269 551	0.015 499	−0.009 309	0.032 666	−0.000 054
0.02	3	1.694 594	0.157 522	0.284 097	0.013 518	−0.008 150	0.033 912	−0.000 023
0.01	3	1.845 055	0.131 821	0.305 512	0.009 926	−0.006 172	0.036 185	−0.000 070
0.008	3	1.889 033	0.123 724	0.312 446	0.008 748	−0.005 479	0.037 970	−0.000 160
0.006	3	1.940 330	0.115 349	0.319 092	0.007 724	−0.004 862	0.038 510	−0.000 149
0.004	3	2.012 234	0.100 881	0.332 352	0.005 316	−0.003 585	0.040 480	−0.000 219
0.002	3	2.114 429	0.083 674	0.348 012	0.002 761	−0.002 235	0.042 473	−0.000 235
0.001	3	2.210 084	0.067 623	0.359 281	0.000 789	−0.000 972	0.042 671	−0.000 177
0.000 5	3	2.294 860	0.051 936	0.372 134	−0.001 437	0.000 414	0.044 705	−0.000 251
0.000 2	3	2.386 346	0.038 200	0.385 234	−0.003 550	0.001 436	0.045 579	−0.000 255
0.000 1	3	2.451 735	0.026 843	0.394 780	−0.005 100	0.002 430	0.047 391	−0.000 346
0.000 05	3	2.512 926	0.015 848	0.404 858	−0.006 836	0.003 427	0.049 353	−0.000 456
0.000 02	3	2.584 356	0.004 341	0.413 512	−0.008 097	0.004 368	0.049 460	−0.000 482
0.000 01	3	2.635 497	−0.004 739	0.421 340	−0.009 380	0.005 190	0.050 504	−0.000 541

shear in u and v and the lidar beam angles from Eq. (12) [$v_{r\text{shr}} = 3.5355$ m s^{-1} km^{-1}];

- calculate the rms radial velocity from shear, s_{shr}, from Eq. (17) [$s_{\text{shr}} = 1.148\ 198$ m s^{-1}];
- calculate the rms velocity s_{vr} from turbulence using Eq. (20), or (22), or (28) [$s_u = 0.0$, $s_v = 1.0732$ m s^{-1}, and $s_w = 0.0$, $s_{vr} = 0.575\ 94$ m s^{-1} from Eq. (28) with a lidar track length $L_{\text{track}} = 100$ km and tropo-

TABLE 3. Coefficients for B (b_{thr}, M, Ω) for $0.25 < \Omega < 2.0$.

b_{thr}	k	a_1	a_2	a_3	a_4	a_5	a_6	a_7
0.7	3	8.980 637	−1.827 780	0.341 578	−0.254 507	0.219 811	−0.261 478	0.012 062
0.6	1	0.267 536	−0.036 049	−0.127 130	−0.020 284	0.010 358	−0.019 788	0.002 029
0.5	1	0.392 329	−0.065 367	−0.085 091	−0.044 156	0.016 104	0.000 483	0.001 609
0.4	1	0.406 278	−0.029 559	−0.123 804	−0.048 936	0.012 910	0.008 251	0.002 497
0.3	1	0.513 703	−0.023 451	−0.183 742	−0.051 110	0.012 966	0.010 376	0.002 572
0.2	1	0.542 020	0.025 307	−0.258 394	−0.051 607	0.008 763	0.043 870	0.001 291
0.1	3	0.713 356	0.080 588	−0.596 139	0.006 109	0.001 928	−0.077 680	0.000 547
0.09	3	0.739 279	0.079 770	−0.594 118	0.005 913	0.001 803	−0.076 013	0.000 456
0.08	3	0.769 235	0.077 517	−0.593 968	0.005 830	0.001 895	−0.074 893	0.000 305
0.07	3	0.780 128	0.090 371	−0.600 091	0.008 286	0.000 059	−0.074 946	0.000 365
0.06	3	0.838 558	0.076 408	−0.586 442	0.005 251	0.001 347	−0.071 629	0.000 226
0.05	3	0.886 049	0.072 054	−0.582 673	0.004 581	0.001 549	−0.070 285	0.000 167
0.04	3	0.924 873	0.077 096	−0.595 487	0.008 050	0.000 520	−0.076 260	0.000 529
0.03	1	1.001 914	0.068 578	−0.548 407	−0.048 873	0.004 249	0.082 415	0.001 372
0.02	1	1.117 766	0.055 385	−0.585 920	−0.053 628	0.006 313	0.095 007	0.001 089
0.01	1	1.229 962	0.070 275	−0.667 194	−0.052 856	0.004 592	0.104 208	0.001 447
0.008	1	1.295 061	0.061 722	−0.689 216	−0.053 937	0.005 552	0.104 605	0.001 676
0.006	1	1.375 680	0.051 883	−0.718 809	−0.054 918	0.006 611	0.103 742	0.002 051
0.004	1	1.453 233	0.047 574	−0.759 126	−0.057 512	0.007 728	0.109 372	0.002 135
0.002	1	1.602 626	0.032 211	−0.816 620	−0.062 789	0.010 044	0.118 020	0.002 541
0.001	1	1.668 114	0.059 734	−0.899 699	−0.059 564	0.006 478	0.121 617	0.003 286
0.000 5	1	1.791 196	0.050 183	−0.949 691	−0.065 593	0.008 072	0.129 993	0.003 904
0.000 2	1	1.946 629	0.035 659	−1.006 546	−0.075 539	0.010 511	0.140 528	0.004 963
0.000 1	1	2.052 813	0.027 336	−1.046 136	−0.083 681	0.012 052	0.147 590	0.005 939
0.000 05	1	2.161 500	0.014 095	−1.074 109	−0.094 529	0.014 335	0.157 808	0.006 901
0.000 02	1	2.297 862	−0.003 658	−1.103 833	−0.110 621	0.017 488	0.171 693	0.008 338
0.000 01	3	2.295 038	0.016 208	−0.587 072	−0.003 916	0.004 788	−0.083 390	0.002 165

Unauthenticated | Downloaded 09/28/21 01:45 AM UTC

TABLE 4. Coefficients for $C(b_{thr}, M, \Omega)$ for $0.25 < \Omega < 2.0$.

b_{thr}	ρ	k	a_1	a_2	a_3	a_4	a_5	a_6	a_7
0.7	0.9	3	−0.429 075	0.201 331	−0.280 863	0.061 607	−0.032 872	0.071 692	−0.000 834
0.6	1.1	3	−0.322 974	0.144 207	−0.239 928	0.054 722	−0.028 373	0.073 233	−0.000 929
0.5	0.9	3	−0.218 434	0.078 202	−0.189 168	0.045 426	−0.022 417	0.077 693	−0.001 066
0.4	0.7	3	−0.124 337	0.008 200	−0.134 713	0.035 085	−0.015 609	0.081 018	−0.001 011
0.3	0.6	3	−0.045 076	−0.066 999	−0.072 603	0.022 493	−0.007 600	0.085 613	−0.000 995
0.2	0.6	3	−0.030 843	−0.125 972	−0.013 707	0.009 435	−0.000 610	0.092 897	−0.001 050
0.1	0.62	3	−0.135 733	−0.157 426	0.031 502	−0.001 604	0.004 173	0.101 428	−0.001 191
0.09	0.62	3	−0.158 431	−0.157 582	0.033 346	−0.002 215	0.004 363	0.101 383	−0.001 137
0.08	0.62	3	−0.183 773	−0.157 738	0.035 593	−0.002 948	0.004 628	0.102 746	−0.001 197
0.07	0.64	3	−0.213 290	−0.156 547	0.038 266	−0.004 000	0.004 768	0.103 767	−0.001 209
0.06	0.64	3	−0.242 714	−0.157 208	0.040 126	−0.004 853	0.005 153	0.104 511	−0.001 234
0.05	0.66	3	−0.286 175	−0.152 208	0.038 909	−0.005 240	0.004 917	0.104 413	−0.001 217
0.04	0.68	3	−0.337 038	−0.147 463	0.036 978	−0.005 325	0.004 803	0.105 213	−0.001 206
0.03	0.7	3	−0.405 277	−0.137 505	0.031 241	−0.004 835	0.004 147	0.104 904	−0.001 182
0.02	0.72	3	−0.487 966	−0.127 783	0.026 408	−0.005 002	0.003 787	0.107 560	−0.001 386
0.01	0.76	3	−0.625 882	−0.107 049	0.009 770	−0.002 892	0.002 347	0.105 259	−0.001 267
0.008	0.78	3	−0.667 207	−0.100 326	0.004 516	−0.002 319	0.001 880	0.104 824	−0.001 276
0.006	0.8	3	−0.713 129	−0.094 790	−0.000 260	−0.001 985	0.001 630	0.104 433	−0.001 257
0.004	0.82	3	−0.785 456	−0.080 175	−0.013 979	0.000 322	0.000 336	0.101 897	−0.001 152
0.002	0.86	3	−0.887 925	−0.063 160	−0.030 785	0.002 675	−0.000 975	0.098 220	−0.000 990
0.001	0.9	3	−0.975 908	−0.052 124	−0.039 446	0.003 383	−0.001 506	0.098 235	−0.001 045
0.000 5	0.92	3	−1.062 552	−0.037 082	−0.051 493	0.005 125	−0.002 701	0.097 138	−0.001 037
0.000 2	0.96	3	−1.156 711	−0.022 534	−0.066 828	0.007 283	−0.003 777	0.094 419	−0.000 979
0.000 1	0.98	3	−1.222 235	−0.011 942	−0.078 327	0.009 109	−0.004 635	0.091 928	−0.000 876
0.000 05	0.98	3	−1.283 708	−0.002 144	−0.088 099	0.010 757	−0.005 423	0.090 710	−0.000 860
0.000 02	1.0	3	−1.359 650	0.013 723	−0.110 548	0.015 056	−0.007 235	0.077 376	0.0
0.000 01	10	3	−1.406 964	0.017 593	−0.107 506	0.013 962	−0.007 052	0.088 187	−0.000 834

spheric conditions with $\epsilon = 2.66 \times 10^{-5}$ m^2 s^{-3}, the 50th percentile of turbulence based on aircraft data (Frehlich 2001a)];
- calculate w_v from lidar pulse width (FWHM) Δt from Eqs. (6) and (7) [$\Delta t = 0.5$ μs; $w_v = 0.374\,788$ m s^{-1}];
- select rms radial velocity jitter σ_{vLO} (m s^{-1}) from LO frequency jitter [$\sigma_{vLO} = 0.5$ m s^{-1}];

TABLE 5. Coefficients for $D(b_{thr}, M, \Omega)$ for $0.25 < \Omega < 2.0$.

b_{thr}	k	a_1	a_2	a_3	a_4	a_5	a_6	a_7
0.7	3	1.563 545	−1.555 591	1.042 268	−0.276 085	0.165 738	−0.669 423	0.027 572
0.6	3	1.940 985	−1.750 224	1.793 081	−0.517 920	0.214 872	−0.256 551	0.026 403
0.5	3	−0.229 436	−0.932 129	1.324 411	−0.429 857	0.134 569	0.053 733	0.010 190
0.4	3	−1.854 910	−0.232 694	0.639 623	−0.279 434	0.055 971	0.164 669	−0.001 622
0.3	3	−2.383 307	0.088 884	0.197 047	−0.178 598	0.013 750	0.181 864	−0.006 112
0.2	3	−1.677 139	−0.089 834	0.153 657	−0.168 262	0.026 109	0.148 657	−0.005 512
0.1	3	−0.607 952	−0.481 262	0.342 257	−0.217 773	0.066 071	0.144 311	−0.005 871
0.09	3	−0.488 586	−0.530 152	0.371 077	−0.224 774	0.071 155	0.141 904	−0.005 625
0.08	3	−0.380 191	−0.574 399	0.421 065	−0.236 676	0.075 805	0.150 442	−0.006 080
0.07	3	−0.146 223	−0.665 988	0.482 935	−0.253 099	0.086 185	0.156 479	−0.006 410
0.06	3	−0.081 104	−0.691 688	0.485 341	−0.254 155	0.088 596	0.141 650	−0.005 499
0.05	3	0.082 169	−0.750 108	0.533 348	−0.266 547	0.095 073	0.142 559	−0.005 494
0.04	3	0.294 660	−0.834 224	0.610 849	−0.286 721	0.104 833	0.157 959	−0.006 436
0.03	3	0.469 714	−0.902 498	0.673 489	−0.302 534	0.112 636	0.162 339	−0.006 480
0.02	3	0.618 769	−0.960 123	0.719 978	−0.315 408	0.118 947	0.149 148	−0.005 760
0.01	3	0.891 298	−1.066 165	0.807 331	−0.341 463	0.132 189	0.154 806	−0.006 728
0.008	3	0.927 231	−1.068 934	0.817 861	−0.345 547	0.132 701	0.155 514	−0.007 090
0.006	3	0.956 619	−1.070 690	0.821 059	−0.347 783	0.133 237	0.153 160	−0.007 172
0.004	3	1.117 476	−1.137 339	0.862 290	−0.360 527	0.141 208	0.145 084	−0.006 975
0.002	3	1.216 180	−1.153 400	0.881 453	−0.367 315	0.143 264	0.138 008	−0.007 051
0.001	3	1.348 018	−1.180 478	0.874 512	−0.369 813	0.146 893	0.121 151	−0.007 085
0.000 5	3	1.434 578	−1.205 783	0.908 692	−0.380 864	0.150 386	0.130 922	−0.008 704
0.000 2	3	1.491 922	−1.187 025	0.874 121	−0.375 736	0.148 049	0.111 899	−0.009 077
0.000 1	3	1.519 028	−1.171 063	0.838 048	−0.368 664	0.145 795	0.091 841	−0.008 853
0.000 05	3	1.509 937	−1.157 015	0.826 269	−0.367 048	0.143 845	0.086 351	−0.009 460
0.000 02	3	1.433 013	−1.066 940	0.545 189	−0.299 570	0.130 119	−0.074 824	0.0
0.000 01	3	1.511 731	−1.112 441	0.743 108	−0.350 065	0.137 929	0.051 964	−0.009 568

Unauthenticated | Downloaded 09/28/21 01:45 AM UTC

TABLE 6. Coefficients for A (b_{thr}, M, Ω) for $2.0 < \Omega < 32.0$.

b_{thr}	k	a_1	a_2	a_3	a_4	a_5	a_6	a_7
0.7	3	−0.753 504	0.557 767	−0.232 905	0.095 772	−0.032 568	−0.029 989	−0.000 356
0.6	3	−0.380 266	0.499 602	−0.073 564	0.071 052	−0.029 379	−0.030 385	−0.000 094
0.5	3	−0.068 962	0.455 845	0.009 627	0.058 087	−0.027 359	−0.025 649	−0.000 021
0.4	2	1.417 021	0.442 154	0.061 470	−0.118 919	0.089 184	0.003 198	0.0
0.3	2	1.881 573	0.396 086	0.111 657	−0.113 497	0.082 353	0.002 868	0.0
0.2	2	2.485 987	0.352 699	0.165 714	−0.107 873	0.069 925	0.002 763	0.0
0.1	2	3.522 915	0.291 163	0.230 597	−0.097 231	0.053 392	0.002 966	0.0
0.09	2	3.673 330	0.283 830	0.244 788	−0.095 610	0.044 322	0.003 399	0.0
0.08	2	3.827 539	0.276 733	0.256 587	−0.094 065	0.039 561	0.003 412	0.0
0.07	2	4.013 603	0.268 285	0.265 886	−0.092 285	0.035 995	0.003 530	0.0
0.06	2	4.239 310	0.256 729	0.281 079	−0.089 359	0.028 420	0.003 803	0.0
0.05	2	4.476 323	0.248 122	0.295 212	−0.087 663	0.021 401	0.004 025	0.0
0.04	2	4.788 753	0.234 167	0.314 925	−0.084 076	0.011 248	0.004 370	0.0
0.03	2	5.163 915	0.217 972	0.351 928	−0.079 133	−0.012 783	0.005 273	0.0
0.02	2	5.634 134	0.201 396	0.384 652	−0.074 484	−0.028 917	0.005 512	0.0
0.01	3	1.877 012	0.108 392	0.361 827	0.003 565	−0.002 995	0.004 114	0.0
0.008	3	1.916 481	0.103 544	0.365 779	0.003 209	−0.002 796	0.004 273	0.0
0.006	3	1.965 835	0.095 006	0.380 509	0.000 740	−0.002 075	0.003 518	0.000 038
0.004	3	2.060 592	0.070 937	0.390 059	−0.001 686	0.000 185	0.007 222	0.0
0.002	3	2.161 597	0.054 586	0.404 980	−0.004 090	0.001 373	0.008 590	0.0
0.001	3	2.257 782	0.035 738	0.422 872	−0.007 556	0.003 071	0.010 441	0.0
0.000 5	3	2.341 957	0.020 043	0.437 777	−0.011 065	0.004 530	0.012 958	0.0
0.000 2	3	2.451 065	−0.002 979	0.455 764	−0.014 557	0.006 656	0.014 800	0.0
0.000 1	3	2.516 766	−0.014 512	0.466 474	−0.016 711	0.007 647	0.016 156	0.0
0.000 05	3	2.582 430	−0.027 619	0.477 379	−0.018 739	0.008 827	0.017 155	0.0
0.000 02	3	2.657 952	−0.041 837	0.490 510	−0.021 615	0.010 155	0.018 955	0.0
0.000 01	3	2.710 315	−0.047 148	0.490 356	−0.018 820	0.009 586	0.016 806	0.0

- calculate w_{veff} from Eqs. (23) and (28) and w_{eff} from Eq. (24) [$w_{veff} = 1.5872$ m s^{-1}; $w_{eff} = 1.5872$ MHz];
- calculate $\Omega = w_{eff} MT_S$ [$\Omega = 11.904$];
- calculate signal level $\Phi_{1thr}(b_{thr}, M, \Omega, N)$ from Eq. (47) at desired threshold b_{thr}[$\Phi_{1thr} = 1.8503$ at $b_{thr} = 0.1$];
- calculate the velocity accuracy of the good estimates $g(b_{thr}, M, \Omega, N)$ from Eq. (48) at the desired threshold b_{thr} [$g = 0.903\ 23$ m s^{-1} at $b_{thr} = 0.1$]; and
- calculate the minimum aerosol backscatter sensitivity using Eq. (5).

The threshold signal level Φ_{1thr} can be calculated with the steps outlined above for coherent Doppler lidars with general lidar parameters and atmospheric conditions. The critical inputs are the turbulence conditions and wind shear. The turbulence level can be selected for tropospheric conditions based on the climatology of turbulence from the Global Atmospheric Research Program (GARP) data (Nastrom and Gage 1985; Frehlich 2001a). The climatology of shear is not well known, especially for the definition of shear used in this work, that is, the best-fit shear to the random velocity over the measurement plane defined by the lidar beam.

b. Producing performance curves

Performance curves $b(\Phi_1)$ and $g(\Phi_1)$ can also be produced from the empirical functions listed in the tables. One possible procedure is to

- calculate the parameters M, Ω, and w_{veff} (previous section);
- calculate $\Phi_{1thr}(b_{thr}, M, \Omega, N)$ for all the values b_{thr};
- calculate the best-fit model $b(\Phi_1)$ using Eq. (41) from tabulated values of $\Phi_{1thr}(b_{thr}, M, \Omega, N)$ and b_{thr};
- calculate $g(b_{thr}, M, \Omega, N)$ for all the values b_{thr};
- calculate the best-fit model $g(\Phi_1)$ using Eq. (42) from tabulated values of $g(b_{thr}, M, \Omega, N)$ and $\Phi_{1thr}(b_{thr}, M, \Omega, N)$; and
- for large Φ_1 set $g(b_{thr}, M, \Omega, N)$ equal to the value $g(b_{thr} = 0.000\ 01, M, \Omega, N)$.

This procedure will produce simple empirical functions for performance. If more accuracy is required, higher-order interpolation of the tabulated values can be used. In addition, simpler models can be used for the best-fit models, for example, a polynomial function for the function $g(\Phi_1, M, \Omega, N)$. An example of the performance curves is shown in Fig. 4 for $\Omega = 2.0$, $M = 100$, and $N = 20$.

9. Sampling error—Troposphere

The sampling errors δ_u and δ_v, as discussed at the end of the introduction, describe how well a chosen measurement system produces a spatial average of the velocity components u and v over each measurement cell. Therefore, this important component of the total observation error [see Eqs. (3) and (4)] depends on the lidar sampling geometry and the spatial statistics of the

Unauthenticated | Downloaded 09/28/21 01:45 AM UTC

TABLE 7. Coefficients for $B(b_{thr}, M, \Omega)$ for $2.0 < \Omega < 32.0$.

b_{thr}	k	a_1	a_2	a_3	a_4	a_5	a_6	a_7
0.7	3	0.000 116	2.816 108	2.408 288	−0.872 208	−0.222 859	0.032 245	0.015 951
0.6	3	0.004 028	1.638 047	−0.251 879	−0.213 702	−0.132 207	−0.004 880	0.006 573
0.5	3	0.036 615	0.890 378	−0.940 341	0.004 912	−0.070 179	−0.014 447	0.002 446
0.4	2	0.045 755	−0.081 214	−0.523 578	3.697 543	−7.827 239	0.972 896	0.0
0.3	3	0.204 779	0.431 332	−1.123 779	0.082 983	−0.033 693	0.005 565	0.0
0.2	2	0.359 162	0.337 506	−0.459 067	−0.107 686	−0.234 442	0.032 294	0.0
0.1	3	0.617 247	0.164 105	−0.769 652	0.033 363	−0.008 668	0.003 002	0.0
0.09	3	0.671 998	0.141 667	−0.759 119	0.033 346	−0.006 684	−0.005 947	0.0
0.08	3	0.721 937	0.127 491	−0.756 387	0.035 249	−0.005 781	−0.009 446	0.0
0.07	2	0.705 292	0.224 593	−0.645 263	−0.086 203	−0.033 058	0.012 174	0.0
0.06	2	0.744 289	0.213 852	−0.551 038	−0.082 323	−0.104 438	0.015 876	0.0
0.05	2	0.795 812	0.193 757	−0.499 818	−0.074 761	−0.133 030	0.016 560	0.0
0.04	2	0.867 370	0.166 193	−0.512 225	−0.062 874	−0.118 766	0.014 544	0.0
0.03	2	0.908 026	0.171 641	−0.442 026	−0.067 554	−0.160 736	0.016 889	0.0
0.02	2	1.081 653	0.109 418	−0.370 387	−0.040 869	−0.236 036	0.021 174	0.0
0.01	3	1.379 920	0.011 531	−0.642 860	0.019 634	0.004 559	−0.009 903	0.0
0.008	3	1.402 501	0.016 804	−0.640 597	0.016 864	0.004 208	−0.004 862	0.0
0.006	3	1.406 311	0.024 646	−0.602 854	0.008 035	0.003 996	−0.006 475	0.000 192
0.004	3	1.426 726	0.035 749	−0.609 022	0.014 288	0.002 155	−0.008 885	0.0
0.002	3	1.568 774	0.021 524	−0.597 032	0.010 680	0.003 750	−0.006 238	0.0
0.001	3	1.686 674	0.013 564	−0.590 200	0.009 018	0.004 596	−0.005 472	0.0
0.000 5	3	1.811 699	0.001 879	−0.582 241	0.009 446	0.005 689	−0.008 646	0.0
0.000 2	3	1.963 383	−0.010 686	−0.571 700	0.006 926	0.007 187	−0.007 909	0.0
0.000 1	3	2.065 523	−0.017 087	−0.566 729	0.005 130	0.007 991	−0.006 682	0.0
0.000 05	3	2.162 955	−0.023 545	−0.561 295	0.003 109	0.008 873	−0.005 235	0.0
0.000 02	3	2.296 191	−0.033 287	−0.556 294	0.002 568	0.009 967	−0.006 327	0.0
0.000 01	3	2.119 740	0.000 688	−0.488 167	−0.033 733	0.009 940	0.028 896	0.0

velocity field. Various sampling patterns were considered by Frehlich (2001a). It is convenient to choose the origin of the measurement cell as the centroid of the lidar pattern and assume the velocity statistics are dominated by the variations over the horizontal plane. Simple results were produced for the troposphere when the forward and aft tracks are overlaid and the wind field statistics are described by a three-dimensional isotropic

TABLE 8. Coefficients for $C(b_{thr}, M, \Omega)$ for $2.0 < \Omega < 32.0$.

b_{thr}	ρ	k	a_1	a_2	a_3	a_4	a_5	a_6	a_7
0.7	0.3	3	−0.956 609	0.397 600	0.015 657	0.019 189	−0.051 753	−0.072 984	0.001 501
0.6	0.25	3	−0.854 518	0.348 444	−0.000 238	0.025 261	−0.049 304	−0.064 549	0.001 299
0.5	0.25	3	−0.644 773	0.248 101	−0.037 190	0.033 566	−0.041 088	−0.044 455	0.000 814
0.4	0.15	3	−0.625 261	0.213 841	−0.063 568	0.043 615	−0.040 451	−0.033 718	0.000 521
0.3	0.4	3	−0.225 523	0.010 767	−0.028 367	0.026 596	−0.016 861	−0.000 396	−0.000 045
0.2	0.5	3	−0.134 716	−0.082 435	0.037 948	0.010 212	−0.005 777	0.010 357	−0.000 131
0.1	0.54	3	−0.218 586	−0.129 566	0.124 470	−0.009 277	0.001 336	0.011 450	0.0
0.09	0.56	3	−0.208 252	−0.141 244	0.111 132	−0.007 768	0.002 654	0.015 450	−0.000 094
0.08	0.57	3	−0.245 276	−0.139 687	0.137 162	−0.012 676	0.002 991	0.011 592	0.000 022
0.07	0.58	3	−0.272 517	−0.139 181	0.138 467	−0.013 364	0.003 156	0.011 799	0.000 024
0.06	0.59	3	−0.283 601	−0.146 786	0.136 389	−0.013 341	0.004 173	0.012 533	0.0
0.05	0.6	3	−0.334 799	−0.139 492	0.140 513	−0.014 891	0.003 792	0.011 971	0.000 033
0.04	0.6	3	−0.373 451	−0.141 379	0.144 157	−0.015 854	0.004 463	0.011 025	0.000 048
0.03	0.61	3	−0.440 219	−0.133 463	0.146 838	−0.017 043	0.004 129	0.009 649	0.000 088
0.02	0.62	3	−0.485 697	−0.135 218	0.116 787	−0.011 619	0.004 418	0.010 824	0.0
0.01	0.63	3	−0.616 967	−0.116 985	0.097 710	−0.009 637	0.003 269	0.010 563	0.0
0.008	0.63	3	−0.694 403	−0.097 945	0.111 768	−0.012 820	0.001 761	0.007 085	0.000 116
0.006	0.63	3	−0.753 263	−0.088 157	0.108 090	−0.012 758	0.001 149	0.006 870	0.000 123
0.004	0.64	3	−0.856 997	−0.060 043	0.096 329	−0.010 479	−0.001 502	0.003 545	0.000 168
0.002	0.65	3	−0.950 661	−0.044 001	0.058 063	−0.003 446	−0.003 009	0.003 513	0.000 097
0.001	0.65	3	−1.059 261	−0.020 842	0.034 258	0.000 301	−0.005 059	0.002 720	0.000 088
0.000 5	0.65	3	−1.139 578	−0.004 510	−0.004 749	0.007 125	−0.006 710	0.004 240	0.0
0.000 2	0.64	3	−1.268 272	0.025 847	−0.031 789	0.012 206	−0.009 632	0.002 062	0.0
0.000 1	0.64	3	−1.355 441	0.046 656	−0.050 165	0.015 161	−0.011 591	0.001 309	0.0
0.000 05	0.64	3	−1.427 900	0.061 536	−0.064 726	0.017 855	−0.012 928	−0.000 003	0.0
0.000 02	0.63	3	−1.531 508	0.086 671	−0.084 652	0.021 903	−0.015 399	−0.001 956	0.0
0.000 01	0.65	3	−1.585 006	0.092 415	−0.086 780	0.019 244	−0.014 818	0.000 211	0.0

Unauthenticated | Downloaded 09/28/21 01:45 AM UTC

TABLE 9. Coefficients for $D(b_{thr}, M, \Omega)$ for $2.0 < \Omega < 32.0$.

b_{thr}	k	a_1	a_2	a_3	a_4	a_5	a_6	a_7
0.7	1	0.891 999	−0.343 770	−0.285 709	0.056 506	0.033 521	0.067 323	−0.002 144
0.6	1	0.731 524	−0.282 538	−0.189 687	0.031 714	0.029 021	0.058 417	−0.001 644
0.5	1	0.628 563	−0.243 698	−0.104 926	0.011 169	0.026 496	0.046 818	−0.001 169
0.4	1	0.510 844	−0.198 054	0.012 698	−0.013 371	0.023 458	0.025 993	−0.000 511
0.3	1	0.404 736	−0.152 076	0.077 324	−0.025 788	0.018 962	0.007 526	0.000 021
0.2	1	0.456 726	−0.157 467	0.084 537	−0.029 485	0.019 316	0.002 602	0.000 197
0.1	1	0.635 261	−0.214 101	0.039 129	−0.027 070	0.024 763	0.016 852	0.0
0.09	1	0.594 904	−0.199 134	0.072 180	−0.034 590	0.023 729	0.013 518	0.000 168
0.08	1	0.621 370	−0.210 353	0.076 537	−0.034 877	0.024 864	0.012 881	0.000 166
0.07	1	0.565 184	−0.183 340	0.081 576	−0.036 499	0.021 991	0.011 052	0.000 253
0.06	1	0.665 708	−0.219 093	0.038 491	−0.030 139	0.025 353	0.021 350	0.0
0.05	1	0.642 486	−0.213 358	0.068 812	−0.035 660	0.025 128	0.017 231	0.000 131
0.04	1	0.645 402	−0.213 267	0.066 290	−0.035 520	0.025 008	0.018 108	0.000 129
0.03	1	0.692 616	−0.229 085	0.038 412	−0.029 583	0.026 179	0.022 216	−0.000 033
0.02	1	0.645 983	−0.213 933	0.059 054	−0.035 463	0.025 233	0.025 144	0.0
0.01	1	0.664 239	−0.224 625	0.065 649	−0.036 975	0.026 541	0.025 483	0.0
0.008	1	0.636 447	−0.215 878	0.084 300	−0.039 411	0.025 709	0.020 817	0.000 101
0.006	1	0.684 387	−0.228 586	0.035 372	−0.028 542	0.026 088	0.025 155	−0.000 125
0.004	1	0.719 350	−0.249 447	0.066 511	−0.034 319	0.028 735	0.021 767	−0.000 014
0.002	3	1.036 765	−1.392 158	1.182 638	−0.416 703	0.177 344	0.139 848	0.000 790
0.001	3	1.130 165	−1.441 528	1.178 119	−0.415 650	0.182 802	0.156 533	0.000 105
0.000 5	3	1.237 563	−1.504 535	1.234 837	−0.416 260	0.189 322	0.141 330	0.0
0.000 2	3	1.255 111	−1.524 850	1.280 990	−0.421 854	0.191 410	0.134 034	0.0
0.000 1	3	1.229 982	−1.517 707	1.321 347	−0.424 477	0.190 579	0.123 345	0.0
0.000 05	3	1.238 847	−1.519 338	1.343 281	−0.426 358	0.190 523	0.117 712	0.0
0.000 02	3	1.221 011	−1.513 333	1.360 459	−0.425 539	0.189 389	0.108 867	0.0
0.000 01	3	1.622 055	−1.626 665	1.131 847	−0.315 573	0.189 941	0.014 615	0.0

Kolmogorov spatial spectrum and the length of the overlaid tracks L_{track} was equal to a square measurement cell $L = L_x = L_y$ (Frehlich 2001a). In general, the track length L_{track} is not equal to the dimensions of the measurement volume.

For the general case of overlaid forward and aft tracks, the sampling error for the along-track component u is given by

$$\delta_u^2 = \langle [u_S - u_{truth}]^2 \rangle, \tag{52}$$

where the average of the velocity component u over the lidar sampling pattern

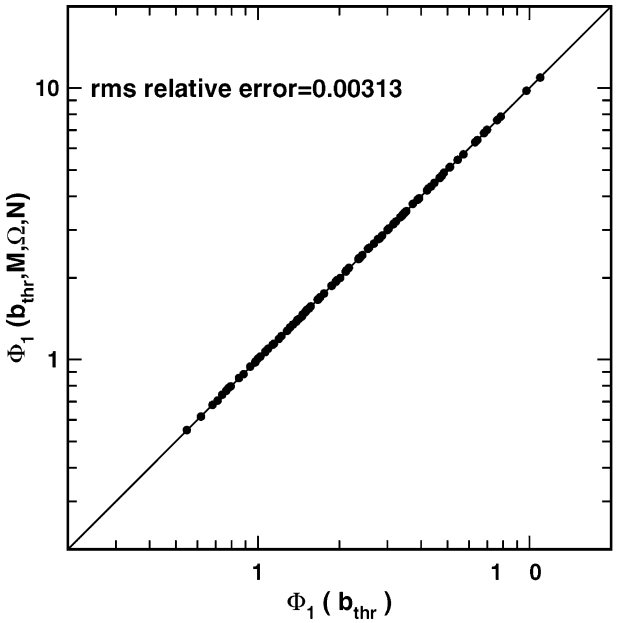

FIG. 2. Comparison of $\Phi_1(b_{thr})$ and model prediction $\Phi_1(b_{thr}, M, \Omega, N)$ for $b_{thr} = 0.1$ and $2.0 < \Omega < 32.0$.

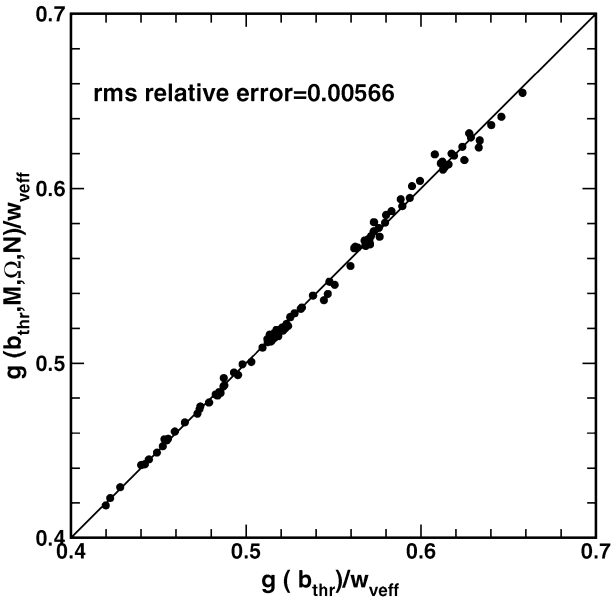

FIG. 3. Comparison of $g(b_{thr})/w_{veff}$ and model prediction $g(b_{thr}, M, \Omega, N)/w_{veff}$ for $b_{thr} = 0.1$ and $2.0 < \Omega < 32.0$.

Unauthenticated | Downloaded 09/28/21 01:45 AM UTC

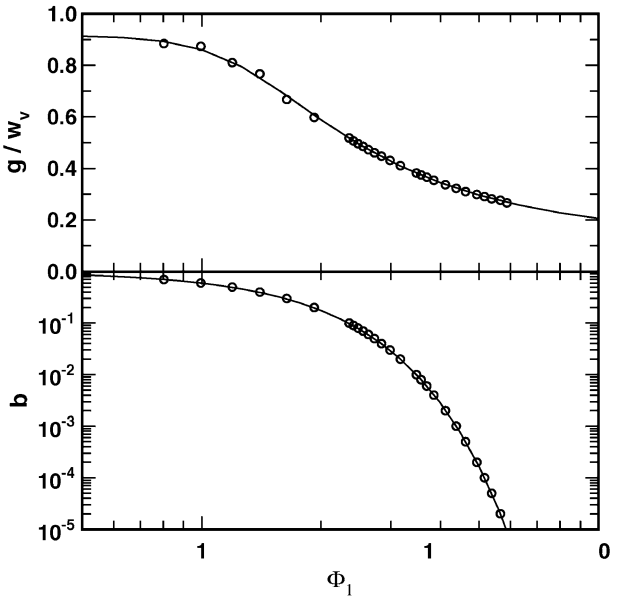

FIG. 4. Performance curves for $M = 100$, $N = 20$, and $\Omega = 2.0$ from the empirical model (circles) and the best-fit model (lines) using Eqs. (40) and (42).

$$u_S = \frac{1}{L_{\text{track}}} \int_{-L_{\text{track}}/2}^{L_{\text{track}}/2} u(x, y = 0)\, dx \quad \text{and} \tag{53}$$

$$u_{\text{truth}} = \frac{1}{L_x L_y} \int_{y=-L_y/2}^{L_y/2} \int_{x=-L_x/2}^{L_x/2} u(x, y)\, dx\, dy \tag{54}$$

is defined as the average of u over the measurement cell and the origin of the coordinate system is chosen as the center of the measurement cell. For homogeneous velocity statistics,

$$\delta_u^2 = \delta_{uc}^2 - \delta_{ut}^2 - s_u^2, \tag{55}$$

where

$$\delta_{uc}^2 = \frac{1}{L_x L_y L_{\text{track}}} \times \int_{-L_x/2}^{L_x/2} \int_{-L_y/2}^{L_y/2} \int_{-L_{\text{track}}/2}^{L_{\text{track}}/2} D_{11}(x - s, y, 0)\, ds\, dy\, dx, \tag{56}$$

$$\delta_{ut}^2 = \frac{1}{L_{\text{track}}} \int_0^{L_{\text{track}}} \left(1 - \frac{x}{L_{\text{track}}}\right) D_{11}(x, 0, 0)\, dx \tag{57}$$

is the mean-square variation of u along the lidar track,

$$s_u^2 = \frac{2}{L_x L_y} \int_0^{L_y} \int_0^{L_x} \left(1 - \frac{x}{L_x}\right)\left(1 - \frac{y}{L_y}\right) D_{11}(x, y, 0)\, dx\, dy \tag{58}$$

is the mean-square variation of u over the measurement volume, and $D_{11}(x, y, z)$ is the structure function of the velocity component u (Monin and Yaglom 1975).

Similarly, the sampling error for the across-track component v, assuming the vertical velocity fluctuations are negligible, is given by

$$\delta_v^2 = \langle [v_S - v_{\text{truth}}]^2 \rangle, \tag{59}$$

where the average of the velocity component v over the lidar sampling pattern

$$v_S = \frac{1}{L_{\text{track}}} \int_{-L_{\text{track}}/2}^{L_{\text{track}}/2} v(x, y = 0)\, dx \quad \text{and} \tag{60}$$

$$v_{\text{truth}} = \frac{1}{L_x L_y} \int_{y=-L_y/2}^{L_y/2} \int_{x=-L_x/2}^{L_x/2} v(x, y)\, dx\, dy \tag{61}$$

is defined as the average of v over the measurement volume. For homogeneous velocity statistics,

$$\delta_v^2 = \delta_{vc}^2 - \delta_{vt}^2 - s_v^2, \tag{62}$$

where

$$\delta_{vc}^2 = \frac{1}{L_x L_y L_{\text{track}}} \times \int_{-L_x/2}^{L_x/2} \int_{-L_y/2}^{L_y/2} \int_{-L_{\text{track}}/2}^{L_{\text{track}}/2} D_{22}(x - s, y, 0)\, ds\, dy\, dx, \tag{63}$$

$$\delta_{vt}^2 = \frac{1}{L_{\text{track}}} \int_0^{L_{\text{track}}} \left(1 - \frac{x}{L_{\text{track}}}\right) D_{22}(x, 0, 0)\, dx \tag{64}$$

is the mean-square variation of v along the lidar track,

$$s_v^2 = \frac{2}{L_x L_y} \int_0^{L_y} \int_0^{L_x} \left(1 - \frac{x}{L_x}\right)\left(1 - \frac{y}{L_y}\right) D_{22}(x, y, 0)\, dx\, dy \tag{65}$$

is the mean-square variation of v over the measurement volume, and $D_{22}(x, y, z)$ is the structure function of the velocity component v (Monin and Yaglom 1975).

The structure functions $D_{11}(x, y, 0)$ and $D_{22}(x, y, 0)$ have been determined from aircraft data for tropospheric conditions by Lindborg (1999). For typical measurement volumes of less than 200 km, a good approximation is given by the Kolmogorov model:

$$D_{11}(r) = \frac{8}{3} \epsilon^{2/3} r^{2/3} \left(1 - \frac{x^2}{4r^2}\right) \quad \text{and} \tag{66}$$

$$D_{22}(r) = \frac{8}{3} \epsilon^{2/3} r^{2/3} \left(1 - \frac{y^2}{4r^2}\right), \tag{67}$$

where ϵ is the energy dissipation rate and $r = \sqrt{x^2 + y^2}$.

Then,

$$\delta_u = (\epsilon L)^{1/3} h_u(L_{\text{track}}/L) \quad \text{and} \tag{68}$$

$$\delta_v = (\epsilon L)^{1/3} h_v(L_{\text{track}}/L), \tag{69}$$

where

Unauthenticated | Downloaded 09/28/21 01:45 AM UTC

$$h_u(x) = 0.687\,592\,1 - 0.372\,358\,1x^{0.717\,261}\exp(0.006\,537\,76\ln^2 x + 0.000\,246\,328\ln^3 x) \quad x < 0.2$$
$$= 0.664\,064\,5\exp(-0.845\,562x + 0.410\,935x^2 - 0.426\,497x^3 + 0.226\,145x^4) \quad 0.2 < x < 0.8$$
$$= 0.350\,945\,0 + 0.276\,700\,3(1-x)^{1.383\,68}\exp[0.086\,612\,7\ln^2(1-x) + 0.006\,796\,48\ln^3(1-x)]$$
$$x > 0.8 \quad \text{and} \quad (70)$$

$$h_v(x) = 0.687\,592\,1 - 0.537\,225\,6x^{0.761\,705}\exp(0.015\,945\,8\ln^2 x + 0.000\,963\,867\ln^3 x) \quad x < 0.2$$
$$= 0.664\,118\,2\exp(-1.295\,13x + 0.824\,060x^2 - 1.534\,97x^3 + 0.845\,310x^4) \quad 0.2 < x < 0.8$$
$$= 0.211\,040\,0 + 0.511\,196\,6(1-x)^{1.682\,86}\exp[0.132\,908\ln^2(1-x) + 0.008\,986\,78\ln^3(1-x)]$$
$$x > 0.8 \quad (71)$$

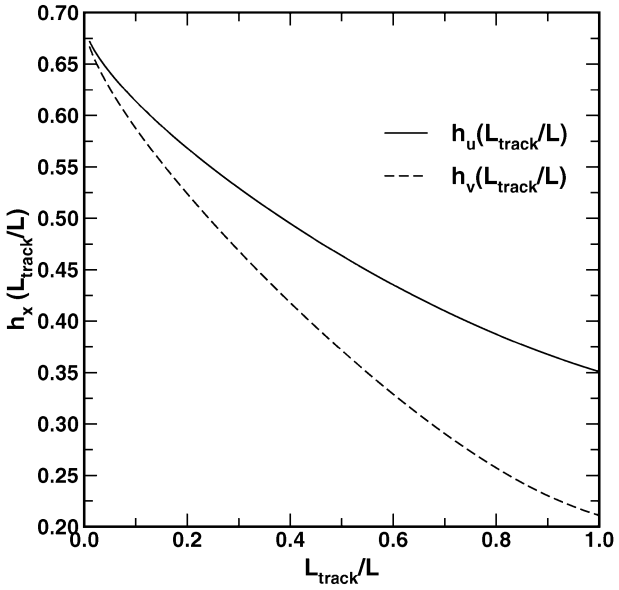

FIG. 5. Sampling error coefficients h_u and h_v as a function of normalized lidar track length L_{track}/L [see Eqs. (68), (69), (70), and (71)].

are approximate empirical functions. The functions $h_u(L_{\text{track}}/L)$ and $h_v(L_{\text{track}}/L)$ are shown in Fig. 5.

10. Summary and discussion

The total random error Σ of Doppler lidar measurements of winds consists of two components: the estimation error σ (sometimes called the instrument error) and the sampling error or error of representativeness δ [Eqs. (3) and (4)]. The estimation error depends on the lidar parameters, the estimation algorithm, and the atmospheric conditions while the sampling error depends on the lidar beam geometry, the definition of the desired measurement or ''truth,'' and the atmospheric conditions such as the statistics of the local turbulence.

For space-based measurements, the most robust geometry is two overlaid forward and aft tracks of multiple lidar shots. The total random errors Σ_u and Σ_v of the along-track and across-track components u and v can be determined from the lidar parameters and the statistics of the atmospheric turbulence. The magnitude σ_u from Eq. (38) and σ_v from Eq. (39) of the estimation error depends on the magnitude σ_e of the total error in the forward and aft radial velocity estimates [see Eqs. (37) and (36)] and are well defined by two parameters: the rms error (standard deviation) g of the good estimates and the fraction b of the random outliers as a function of the signal energy Φ_1. When the lidar signal is weak and random otuliers are produced, it is important to include the statistical properties of the parameter $d = v_0 - v_{\text{truth}}$, the difference between the center of the velocity search space v_0 and the desired radial velocity measurement v_{truth}. For high-signal levels, $b = 0$ and only the parameter g is required for predicting the estimation errors.

For coherent Doppler lidar performance in the weak-signal regime with pulse accumulation, the predictions of the effective Gaussian signal model agree with the full simulations that include realistic wind and aerosol backscatter variability (see Fig. 1). This is the typical scenario for space-based operation and for ground-based operation using high PRF solid-state lidars. The empirical functions produced for threshold signal levels using this approximation are accurate over a large parameter space and therefore the analysis for general conditions is reduced to four basic input variables: the threshold criteria b_{thr}, the number of complex data points M collected per range gate, the number N of lidar pulses accumulated per radial velocity estimate, and the normalized spectral width $\Omega = w_{\text{eff}}\,MTs$ from Eq. (25), which is also written in terms of $w_{v\text{eff}}$, from Eq. (23), the effective signal spectral width in velocity space. Since for space-based measurements $w_{v\text{eff}}$ is usually dominated by the wind field turbulence ($s_{v\text{eff}} > w_v$), the predictions of performance require the statistical description of the atmospheric wind field or, more precisely, the total wind variability $s_{v\text{eff}}$ from Eq. (15) over the lidar measurement plane, which consists of [see Eq. (16)] a wind shear component s_{shr} using Eq. (17) and a turbulent component s_{vr} using Eqs. (18), (20), or (22). For tropospheric conditions and Kolmogorov turbulence s_{vr} is given by Eqs. (28), (30), and (31) in terms of the single turbulence parameter ϵ, the energy dissipation

Unauthenticated | Downloaded 09/28/21 01:45 AM UTC

rate. In the boundary layer, s_{vr} can be calculated assuming a von Kármán spectrum [see Eqs. (28), (32), (33), and (34)].

The threshold signal level $\Phi_{1\text{thr}}$ for the chosen fraction b_{thr} of the random outliers is calculated with the empirical functions in section 7. A user's manual is provided in section 8a to guide the user in the calculation of the input parameters. The wind variability component from turbulence s_{vr} is the most difficult parameter to accurately specify. More research is required to determine the statistical description and the climatology of atmospheric turbulence. A user's manual is also provided in section 8b to calculate performance curves of the radial velocity estimates as a function of the signal level Φ_1 based on the table of coefficients of the empirical functions.

The performance curves $b(\Phi_1)$ and $g(\Phi_1)$ describe the magnitude σ_e using Eqs. (37) and (36) of the random estimation error of the radial velocity estimates as well as the magnitude of the random estimation error of the estimates of u and v from overlaid forward and aft lidar tracks [see Eqs. (38) and (39)]. The calculation of the total observation error Σ of the estimates of u and v requires a calculation of the sampling error or error of representativeness δ [Eqs. (3) and (4)], which depends on the lidar sampling pattern and the statistical description of the atmospheric turbulence. For two overlaid forward and aft lidar tracks and Kolmogorov turbulence, simple scaling laws are produced in terms of the lidar track length L_{track} and the dimensions L of a square measurement cell for tropospheric conditions [see Eqs. (68) and (69)]. These calculations of total observation error for estimates of u and v are critical for defining data requirements, providing verification with other independent measurements (Frehlich 2001a), optimizing data assimilation algorithms and forecast models, and producing realistic observing system simulation experiments (Rohaly and Krishnamurti 1993; Baker et al. 1995; Atlas 1997).

Acknowledgments. This work was supported by two grants from the National Aeronautics and Space Administration, Langley Space Flight Center, Michael J. Kavaya and Syed Ismail, technical officers. The author acknowledges useful discussions with Michael Kavaya, Dave Emmitt, and Bob Sharman.

REFERENCES

Anderson, J. R., 1991: High performance velocity estimators for coherent laser radars. *Sixth Topical Meeting on Coherent Laser Radar: Technology and Applications*, Snowmass-at-Aspen, CO, Optical Society of America, 216–218.

Atlas, R., 1997: Atmospheric observations and experiments to assess their usefulness in data assimilation. *J. Meteor. Soc. Japan,* **75,** 111–130.

Baker, W. E., and Coauthors, 1995: Lidar measured winds from space: An essential component for weather and climate prediction. *Bull. Amer. Meteor. Soc.,* **76,** 869–888.

Belan, B. D., A. I. Grishin, G. O. Zadde, and G. G. Matviyenko, 1987: Correlation functions and spectral densities of aerosol concentration and of fluctuations in the aerosol backscatter coefficient in the lower atmosphere. *Atmos. Oceanic Phys.,* **23,** 301–305.

Bowdle, D. A., 1997: Aerosol backscatter spatial structure: Preliminary results. University of Alabama in Huntsville Rep. to NASA Dryden Flight Research Center, Contract NCC8-22, 41 pp.

Frehlich, R. G., 1993: Coherent Doppler lidar signal covariance including wind shear and wind turbulence. *Appl. Opt.,* **33,** 6472–6481.

——, 1996: Simulation of coherent Doppler lidar performance in the weak signal regime. *J. Atmos. Oceanic Technol.,* **13,** 646–658.

——, 1997: Effects of wind turbulence on coherent Doppler lidar performance. *J. Atmos. Oceanic Technol.,* **14,** 54–75.

——, 2000: Simulation of coherent Doppler lidar performance for space-based platforms. *J. Appl. Meteor.,* **39,** 245–262.

——, 2001a: Errors for space-based Doppler lidar wind measurements: Definition, performance, and verification. *J. Atmos. Oceanic Technol.,* **18,** 1749–1772.

——, 2001b: Estimation of velocity error for Doppler lidar measurements. *J. Atmos. Oceanic Technol.,* **18,** 1628–1639.

——, and M. J. Yadlowsky, 1994: Performance of mean frequency estimators for Doppler radar and lidar. *J. Atmos. Oceanic Technol.,* **11,** 1217–1230; Corrigendum, **12,** 445–446.

——, S. Hannon, and S. Henderson, 1994: Performance of a 2-μm coherent Doppler lidar for wind measurements. *J. Atmos. Oceanic Technol.,* **11,** 1517–1528.

——, ——, and ——, 1997: Coherent Doppler lidar measurements of winds in the weak signal regime. *Appl. Opt.,* **36,** 3491–3499.

——, ——, and ——, 1998: Coherent Doppler lidar measurements of wind field statistics. *Bound.-Layer Meteor.,* **86,** 233–256.

Henderson, S. W., C. P. Hale, J. R. Magee, M. J. Kavaya, and A. V. Huffaker, 1991: Eye-safe coherent laser radar system at 2.1 μm using Tm,Ho:YAG lasers. *Opt. Lett.,* **16,** 773–775.

——, P. J. M. Suni, C. P. Hale, S. M. Hannon, J. R. Magee, D. L. Bruns, and E. H. Yuen, 1993: Coherent laser radar at 2 μm using solid-state lasers. *IEEE Trans. Geosci. Remote Sens.,* **31,** 4–15.

Huffaker, M. R., and R. M. Hardesty, 1996: Remote sensing of atmospheric wind velocities using solid-state and CO_2 coherent laser systems. *Proc. IEEE,* **84,** 181–204.

——, T. R. Lawrence, M. J. Post, J. T. Priestley, F. F. Hall Jr., R. A. Richter, and R. J. Keeler, 1984: Feasibility studies for a global wind measuring satellite system (Windsat): Analysis of simulated performance. *Appl. Opt.,* **23,** 2523–2536.

Kavaya, M. J., S. W. Henderson, J. R. Magee, C. P. Hale, and R. M. Huffaker, 1989: Remote wind profiling with a solid-state Nd: YAG coherent lidar system. *Opt. Lett.,* **14,** 776–778.

Lindborg, E., 1999: Can the atmospheric kinetic energy spectrum be explained by two-dimensional turbulence? *J. Fluid Mech.,* **388,** 259–288.

Marple, S. L., Jr., 1987: *Digital Spectral Analysis with Applications.* Prentice-Hall, 492 pp.

Menzies, R. T., 1986: Doppler lidar atmospheric wind sensors: A comparative performance evaluation for global measurement applications from earth orbit. *Appl. Opt.,* **25,** 2546–2553.

——, and R. M. Hardesty, 1989: Coherent Doppler lidar for measurements of wind fields. *Proc. IEEE,* **77,** 449–462.

Monin, A. S., and A. M. Yaglom, 1975: *Statistical Fluid Mechanics: Mechanics of Turbulence.* Vol. 2. The MIT Press, 874 pp.

Nastrom, G. D., and K. S. Gage, 1985: A climatology of atmospheric wavenumber spectra of wind and temperature observed by commercial aircraft. *J. Atmos. Sci.,* **42,** 950–960.

Osipenko, F. P., A. P. Chaykovskiy, and V. N. Shcherbakov, 1989: Microstructure variations and statistical characteristics of the backscatter index of the aerosol in the atmospheric boundary layer as indicated by multifrequency soundings. *Atmos. Oceanic Phys.,* **25,** 528–532.

Press, W. H., B. P. Flannery, S. A. Teukolsky, and W. T. Vetterling, 1986: *Numerical Recipes: The Art of Scientific Computing.* Cambridge University Press, 818 pp.

Unauthenticated | Downloaded 09/28/21 01:45 AM UTC

Rohaly, G., D., and T. N. Krishnamurti, 1993: An observing system simulation experiment for the Laser Atmospheric Wind Sounder (LAWS). *J. Appl. Meteor.,* **32,** 1452–1471.

Rothermel, J., D. A. Bowdle, J. M. Vaughan, and M. J. Post, 1989: Evidence of a tropospheric aerosol backscatter background mode. *Appl. Opt.,* **28,** 1040–1042.

——, ——, and V. Srivastava, 1996: Mid-tropospheric aerosol backscatter background mode over the Pacific Ocean at 9.1 μm wavelength. *Geophys. Res. Lett.,* **23,** 281–284.

Rye, B. J., 1990: Spectral correlation of atmospheric lidar returns with range-dependent backscatter. *J. Opt. Soc. Amer.,* **7A,** 2199–2207.

——, and R. M. Hardesty, 1993a: Discrete spectral peak estimation in incoherent backscatter heterodyne lidar. I. Spectral accumulation and the Cramer–Rao lower bound. *IEEE Trans. Geosci. Remote Sens.,* **31,** 16–27.

——, and ——, 1993b: Discrete spectral peak estimation in incoherent backscatter heterodyne lidar. II. Correlogram accumulation. *IEEE Trans. Geosci. Remote Sens.,* **31,** 28–35.

Salamitou, P., A. Dabas, and P. H. Flamant, 1995: Simulation in the time domain for heterodyne coherent laser radar. *Appl. Opt.,* **34,** 499–506.

Unauthenticated | Downloaded 09/28/21 01:45 AM UTC